Title

Effects of MicroRNA-34a on the Pharmacokinetics of Cytochrome P450 Probe Drugs in Mice

Journal

Drug Metabolism and Disposition, 45(5)

ISSN

0090-9556

Authors

Jilek, Joseph L
Tian, Ye
Yu, Ai-Ming

Publication Date

2017-05-01

DOI

10.1124/dmd.116.074344

Peer reviewed

1521-009X/45/5/512–522$25.00
Drug Metabolism and Disposition
https://doi.org/10.1124/dmd.116.074344
Drug Metab Dispos 45:512–522, May 2017

Effects of MicroRNA-34a on the Pharmacokinetics of Cytochrome P450 Probe Drugs in Mice

Joseph L. Jilek, Ye Tian, and Ai-Ming Yu

Department of Biochemistry and Molecular Medicine, Comprehensive Cancer Center, University of California Davis School of Medicine, Sacramento, California (J.L.J., Y.T., A.-M.Y.); and Key Laboratory for Space Bioscience and Biotechnology, Institute of Special Environmental Biophysics, School of Life Sciences, Northwestern Polytechnical University, Xi'an, Shaanxi, China (Y.T.)

Received November 20, 2016; accepted March 1, 2017

ABSTRACT

MicroRNAs (miRNAs or miRs), including miR-34a, have been shown to regulate nuclear receptor, drug-metabolizing enzyme, and transporter gene expression in various cell model systems. However, to what degree miRNAs affect pharmacokinetics (PK) at the systemic level remains unknown. In addition, miR-34a replacement therapy represents a new cancer treatment strategy, although it is unknown whether miR-34a therapeutic agents could elicit any drug–drug interactions. To address this question, we refined a practical single-mouse PK approach and investigated the effects of a bioengineered miR-34a agent on the PK of several cytochrome P450 probe drugs (midazolam, dextromethorphan, phenacetin, diclofenac, and chlorzoxazone) administered as a cocktail. This approach involves manual serial blood microsampling from a single mouse and requires a sensitive liquid chromatography–tandem mass spectrometry assay, which was able to illustrate the sharp changes in midazolam PK by ketoconazole and pregnenolone 16α-carbonitrile as well as phenacetin PK by α-naphthoflavone and 3-methylcholanthrene. Surprisingly, 3-methylcholanthrene also decreased systemic exposure to midazolam, whereas both pregnenolone 16α-carbonitrile and 3-methylcholanthrene largely reduced the exposure to dextromethorphan, diclofenac, and chlorzoxazone. Finally, the biologic miR-34a agent had no significant effects on the PK of cocktail drugs but caused a marginal (45%–48%) increase in systemic exposure to midazolam, phenacetin, and dextromethorphan in mice. In vitro validation of these data suggested that miR-34a slightly attenuated intrinsic clearance of dextromethorphan. These findings from single-mouse PK and corresponding mouse liver microsome models suggest that miR-34a might have minor or no effects on the PK of coadministered cytochrome P450–metabolized drugs.

Introduction

MicroRNAs (miRNAs or miRs) are a family of short, noncoding RNAs that govern various cellular processes through post-transcriptional regulation of target gene expression (Ambros, 2004). Recent studies have demonstrated that many miRNAs are able to modulate the expression of nuclear receptors, drug-metabolizing enzymes, and transporters and consequently alter cellular drug metabolism and disposition capacities (Yu, 2009; Ingelman-Sundberg et al., 2013; Yokoi and Nakajima, 2013; Yu et al., 2016). As an example, miR-34a was shown to directly regulate hepatocyte nuclear factor 4α (HNF4α or NR2A1) (Takagi et al., 2010), 9-*cis* retinoic acid receptor α (RXRα or NR2B1) (Oda et al., 2014), and nuclear factor (erythroid-derived 2)–like 2 (Nrf2 or NFE2L2) (Huang et al., 2014) in a number of cell line models. In addition, a negative correlation between CYP3A4 and miR-34a levels in a set of human liver samples was also identified (Lamba et al., 2014). Nevertheless, it is unknown to what levels miRNAs may affect the pharmacokinetic (PK) properties of a drug in a whole body system.

As master regulators of gene expression behind disease development and progression, some miRNAs may serve as therapeutic targets or agents (Bader et al., 2010; Kasinski and Slack, 2011; Ho and Yu, 2016). Among them, miR-34a is commonly downregulated in patient tumor tissues and acts as a tumor suppressor (for a review, see Bader, 2012). Therefore, miR-34a agents may be reintroduced into tumor cells to control tumor progression and metastasis. Recently, our group bioengineered a chimeric miR-34a agent and demonstrated that this biologic miR-34a prodrug is effective to suppress miR-34a target gene expression, inhibit human carcinoma cell proliferation and invasion, and reduce tumor growth in subcutaneous and orthotopic xenograft mouse models (Wang et al., 2015; Zhao et al., 2015, 2016). However, it is unknown whether therapeutic miR-34a would cause significant drug–drug interactions (DDIs), which are a critical component in drug development, particularly for combination therapy.

A robust and relevant in vivo system is warranted for assessing PK DDIs, rather than predictions using in vitro data. However, preclinical PK DDI studies have largely been limited to the use of larger animal

This research was supported by the National Institutes of Health National Institute of General Medical Sciences [Grant R01GM133888 and Pharmacology Training Program Grant T32GM099608 (to J.L.J.)] and the National Institutes of Health National Cancer Institute [Grant U01CA175315].

J.L.J. and Y.T. contributed equally to this work.

https://doi.org/10.1124/dmd.116.074344.

ABBREVIATIONS: 1′-OH-MDZ, 1′-hydroxymidazolam; 3-MC, 3-methylcholanthrene; 4′-OH-DIC, 4′-hydroxydiclofenac; 6-OH-CLZ, 6-hydroxychlorzoxazone; α-NF, α-naphthoflavone; APAP, acetaminophen; AUC, area under the plasma drug concentration versus time curve; CL_{int}, intrinsic clearance; CLZ, chlorzoxazone; DDI, drug–drug interaction; DIC, diclofenac; DXM, dextromethorphan; DXO, dextrorphan; ESI, electrospray ionization; HNF, hepatocyte nuclear factor; KTZ, ketoconazole; LC, liquid chromatography; MDZ, midazolam; miR, microRNA; miRNA, microRNA; MS, mass spectrometry; MS/MS, tandem mass spectrometry; MSA, methionine-Sephadex aptamer; P450, cytochrome P450; PCN, pregnenolone-16α-carbonitrile; PHE, phenacetin; PK, pharmacokinetics; RXR, 9-*cis* retinoic acid receptor; $t_{1/2}$, elimination half-life; tRNA, transfer RNA.

species, such as rats, canines, and nonhuman primates. A major barrier to the use of mice for PK studies is attributable to the need for large volumes of blood collected at a sufficient number of individual time points to construct a robust, single-animal plasma drug concentration-time curve. As such, the use of mice in PK DDI studies has traditionally been limited to a "giant rat" approach, in which individual mice are bled only at one to three time points and thus different mice are used to generate a complete blood drug concentration-time profile for naïve-pooled population PK analysis and modeling (Granvil et al., 2003; Shen et al., 2011; Jiang et al., 2013). This method is valid given a robust analytical technique; however, intraindividual variability may manifest in exacerbated interanimal variation in the PK profile and estimated PK parameters, ultimately compromising statistical power.

To delineate the potential effects of miR-34a on the PK of coadministered drugs or possible DDIs, we first established a new practical single-mouse PK approach, requiring only simple manual blood microsampling via the mouse tail vein coupled to a sensitive and accurate liquid chromatography (LC)–tandem mass spectrometry (MS/MS) assay. This LC-MS/MS assay allowed simultaneous quantification of five major cytochrome P450 (P450) probe drugs and corresponding metabolites in minimal sample matrix. Complete plasma drug concentration-time curves in mice were thus successfully constructed and used for PK analyses. The validity and utility of this single-mouse PK approach was further demonstrated by the sharp effects of selective P450 inhibitors and inducers on corresponding P450 probe drugs. Using this single-mouse PK approach, we thus successfully defined the effects of miR-34a on the PK of individual P450 probe drugs.

Materials and Methods

Chemicals and Reagents. Chlorzoxazone (CLZ), α-naphthoflavone (α-NF), harmaline hydrochloride, 6-hydroxychlorzoxazone (6-OH-CLZ), ketoconazole (KTZ), 3-methylcholanthrene (3-MC), pregnenolone-16α-carbonitrile (PCN), phenacetin (PHE), and warfarin sodium were purchased from Sigma-Aldrich (St. Louis, MO). Acetaminophen (APAP) and EDTA were purchased from MP Biomedicals LLC (Aurora, OH). Dextromethorphan (DXM) hydrobromide and dextrorphan (DXO) were purchased from ICN Biomedicals Inc. (Aurora, OH). Diclofenac (DIC) sodium was purchased from TCI America (Portland, OR). Midazolam (MDZ) was purchased from Cambridge Isotope Laboratories (Tewksbury, MA). 1′-Hydroxymidazolam (1′-OH-MDZ) was purchased from Bertin Pharma (Montigny le Bretonneux, France). 4′-Hydroxydiclofenac (4′-OH-DIC) was purchased from Toronto Research Chemicals Inc. (Toronto, ON, Canada). Blank CD-1 mouse plasma (with EDTA) was purchased from BioreclamationIVT (Baltimore, MD). Sterile phosphate-buffered saline (pH 7.4) was purchased from Gibco (Grand Island, NY). LC/mass spectrometry (MS)–grade acetonitrile, methanol, and formic acid were purchased from Fisher Scientific (Fair Lawn, NJ). In vivo jetPEI was purchased from Polyplus Transfection (Illkirch, France).

The P450 probe substrate cocktail consisted of MDZ, PHE, DXM, DIC, and CLZ, and the stock solutions were dissolved in dimethylsulfoxide. An appropriate dosing formulation was prepared by diluting the stock solutions in phosphate-buffered saline for a dosage volume of 0.6 ml/30 g body weight and specific dose of 1.0 mg/kg MDZ, 2.8 mg/kg PHE, 26 mg/kg DXM, 3.25 mg/kg DIC, and 6.5 mg/kg CLZ.

Expression and Purification of RNA Agents. Recombinant miR-34a prodrug and the control transfer RNA (tRNA)/methionine-Sephadex aptamer (MSA) were prepared as previously described (Wang et al., 2015). Briefly, competent HST08 *Escherichia coli* bacteria were transformed with appropriate plasmids; after a 12-hour incubation at 37°C, bacteria were pelleted, resuspended, lysed in phenol to extract total RNA, and precipitated with salt and ethanol. Target RNA was isolated from total RNAs by an anion exchange fast protein LC method using an NGC FPLC system (Bio-Rad, Hercules, CA), and its purity (>99%, data not shown) was verified by a high-performance LC assay (Wang et al., 2015).

Animals, Drug Administration, and Serial Blood Microsampling. All animal procedures were approved by the Institutional Animal Care and Use Committee at University of California Davis and were carried out in accordance with the 2015 U.S. Department of Health and Human Services Guide for the Care and Use of Laboratory Animals. Male CD-1 mice aged 4–6 weeks (approximately 30 g bodyweight) were purchased from Charles River Laboratories (Hollister, CA), housed under 12-hour light/dark conditions, and provided with diet and water ad libitum.

Mice were administered either KTZ (50 mg/kg) or α-NF (100 mg/kg) or vehicle (corn oil) (six mice per group) intraperitoneally to assess the impact of the P450 inhibitor on probe drug PK. After 1 hour, mice were given a P450 probe substrate cocktail by oral gavage at specific doses outlined above. Immediately after cocktail administration, manual microsampling was conducted at the following time points: 3, 10, 20, 30, 45, 50, 90, 120, and 180 minutes. Specifically, a small volume of blood (10–20 μl) was collected by carefully inserting a 28-gauge needle precoated with 6% EDTA into the lateral tail vein of a mouse restrained by a mouse holder during blood collection (Fig. 1), and mice were returned to their cages in between sampling time points. Mice were euthanized right after the experiment, and separate batches of mice were used for the KTZ, α-NF, and vehicle treatment groups. Blood was then transferred into a 1.5-ml microcentrifuge tube containing 1 μl 6% EDTA and was centrifuged at

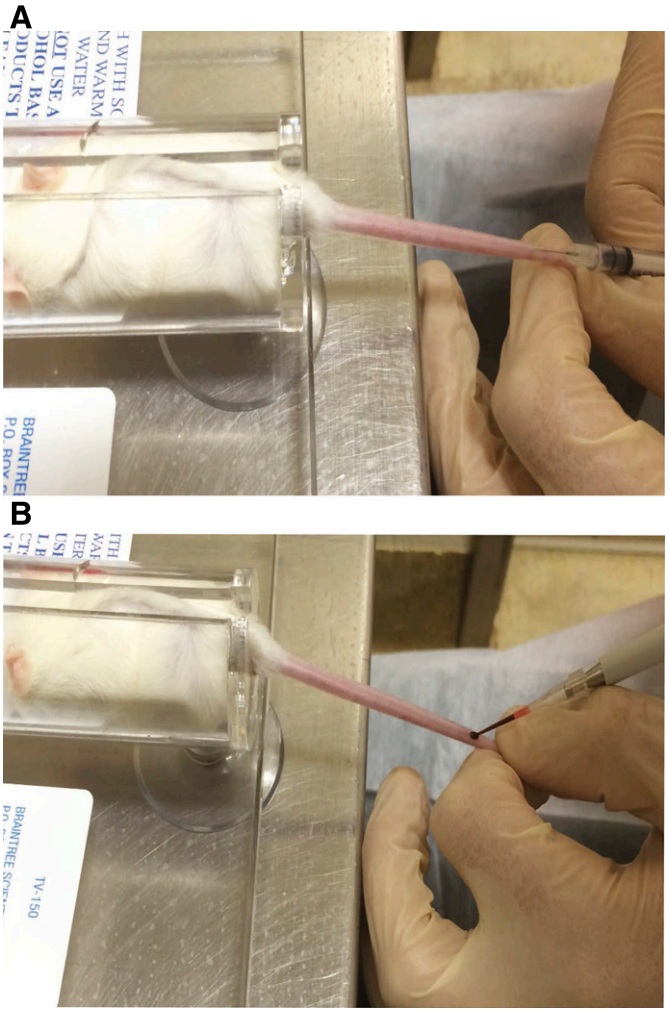

Fig. 1. Serial blood microsampling from a single mouse. The mouse was restrained using a cylinder, allowing free access to the tail. (A) Using a 30-gauge needle, the lateral tail vein was pierced at an angle similar to intravenous injection into the tail vein. The plunger of the syringe was slightly aspirated, the needle was quickly removed, and a large drop of blood was allowed to form, using pressure to draw blood to the site of puncture if necessary. (B) The drop of blood was quickly collected using a 10-μl pipette tip (previously coated with 6% EDTA), transferred to a microcentrifuge tube containing 1 μl 6% EDTA, and placed on ice until centrifugation.

TABLE 1

ESI-MS/MS conditions and calibration ranges for individual analytes

Analyte	Retention Time	ESI Mode	MRM Transition	Scan Time	DP	CE	CXP	Calibration Range
	min		*Da*	*ms*		*V*		*nM*
PHE	5.81	Positive	180.0 → 110.1	150	61	29	8	25–5000
APAP	1.26	Positive	152.1 → 110.1	130	41	27	8	5–1000
DXM	7.13	Positive	272.3 → 171.1	150	91	57	14	25–5000
DXO	4.33	Positive	258.2 → 157.0	100	51	53	12	5–1000
MDZ	6.97	Positive	326.7 → 292.1	150	81	41	8	5–1000
1′-OH-MDZ	7.34	Positive	342.0 → 203.0	150	51	35	10	25–5000
Harmaline (IS)	4.89	Positive	215.2 → 172.1	110	36	43	16	NA
DIC	6.93	Negative	294.0 → 249.8	300	−55	−16	−5	25–5000
4′-OH-DIC	6.50	Negative	309.9 → 265.7	200	−55	−16	−7	5–1000
CLZ	5.28	Negative	167.8 → 131.9	200	−60	−28	−5	25–5000
6′-OH-CLZ	3.64	Negative	183.8 → 119.9	150	−55	−26	−7	5–1000
Warfarin (IS)	6.57	Negative	306.8 → 160.9	100	−60	−28	−11	NA

Analytes were separated on a C18 column prior to positive or negative ESI MRM of each analyte. Calibrators were standard drugs and metabolites spiked in blank CD-1 mouse plasma and processed as described in the *Materials and Methods*. CE, collision energy; CXP, collision cell exit potential; DP, declustering potential; IS, internal standard; MRM, multiple reaction monitoring; NA, calibration range not applicable to internal standards.

5000 rpm and 4°C for 10 minutes. Plasma was transferred into a clean microcentrifuge tube and stored at −80°C until LC-MS/MS quantification.

Likewise, different batches of mice were used to examine the P450 inducer (six mice per group) on the PK of P450 probe drugs, which were administered intraperitoneally with either PCN (40 mg/kg), 3-MC (50 mg/kg), or vehicle (corn oil) once daily for 3 days. Cocktail administration and blood collection were conducted 24 hours after the treatment with the P450 inducer or vehicle and were performed in the same manner as the inhibition study.

To assay the effects of miR-34a on systemic PK, a paired study design was followed using a separate cohort of mice, which would improve statistical power. Mice were first administered in vivo jetPEI-formulated tRNA/MSA intravenously (15 μg RNA daily for 4 consecutive days). Twenty-four hours after the last dose of RNA agent, mice were treated with the P450 probe drug cocktail and blood samples were collected as described above. After a 2-week washout and recovery period (U.S. Department of Health and Human Services, https://oacu.oir.nih.gov/animal-research-advisory-committee-guidelines), the same mice were injected with the miR-34a prodrug using the same dose and regimen, followed by the PK study.

To examine the levels of miR-34a accumulation in the mouse liver and the impact on hepatic drug-metabolizing capacity, a separate batch of male CD-1

TABLE 2

Intra- and interday precision and accuracy for LC-MS/MS quantification of P450 probe drugs and corresponding metabolites in mouse plasma

Concentrations are given in nanomoles. Values represent means ± S.D. or percentages unless otherwise indicated.

Analyte	Nominal Concentration	Intra-assay (n = 3)			Interassay (n = 9)		
		Measured Concentration	Relevant S.D.	Accuracy	Measured Concentration	Relevant S.D.	Accuracy
PHE	75	69.93 ± 18.70	26.7	93.2	75.69 ± 10.84	14.3	101
	400	387.7 ± 20.8	5.38	96.8	394.9 ± 15.4	3.89	98.6
	4000	3580 ± 114	3.17	89.4	3707 ± 168	4.54	92.6
APAP	15	14.97 ± 1.85	12.4	99.9	15.69 ± 1.23	7.84	104
	80	81.57 ± 0.96	1.18	102	78.96 ± 2.38	3.02	98.7
	800	699.7 ± 11.8	1.69	87.4	722.6 ± 36.5	5.05	90.3
MDZ	15	15.40 ± 1.95	12.7	103	14.63 ± 1.98	13.6	97.5
	80	73.77 ± 5.13	6.95	92.2	77.96 ± 9.29	11.9	97.4
	800	688.7 ± 66.3	9.62	86.1	721.3 ± 57.2	7.93	90.2
1′-OH-MDZ	75	71.47 ± 3.50	4.90	95.4	74.56 ± 6.18	8.29	99.4
	400	382.3 ± 23.0	6.02	95.6	378.0 ± 14.4	3.80	94.5
	4000	3523 ± 136	3.86	88.1	3661 ± 272	7.42	91.6
DXM	75	64.67 ± 10.80	16.7	83.0	66.46 ± 7.47	11.2	87.5
	80	356.0 ± 14.7	4.14	89.0	371.8 ± 19.6	5.27	92.9
	800	3767 ± 186	4.93	94.2	3741 ± 161	4.29	93.6
DXO	15	12.67 ± 2.63	20.7	84.6	12.87 ± 2.14	16.7	85.8
	400	67.90 ± 4.48	6.60	84.9	72.92 ± 5.45	7.48	91.1
	4000	700.0 ± 25.9	3.71	87.5	736.8 ± 39.4	5.35	92.1
DIC	75	86.20 ± 6.77	7.86	115	90.33 ± 21.56	23.9	121
	400	468.3 ± 11.2	2.40	117	421.8 ± 48.6	11.5	106
	4000	3647 ± 123	3.38	91.1	4148 ± 604	14.6	104
4′-OH-DIC	15	15.70 ± 2.48	15.8	105	17.61 ± 3.02	17.2	118
	80	86.87 ± 15.76	18.2	109	81.39 ± 12.65	15.6	102
	800	826.3 ± 20.2	2.45	103	876.6 ± 102.8	11.7	110
CLZ	75	87.60 ± 8.88	10.1	117	92.79 ± 16.50	17.8	124
	400	429.3 ± 51.6	12.0	107	413.4 ± 52.2	12.6	103
	4000	3716 ± 311	8.36	92.9	4290 ± 700	16.3	107
6′-OH-CLZ	15	16.33 ± 4.71	28.8	109	16.64 ± 3.60	21.6	111
	80	84.17 ± 14.1	16.8	105	81.91 ± 34.78	12.8	116
	800	678.3 ± 157.8	23.3	84.8	840.1 ± 194.5	23.2	105

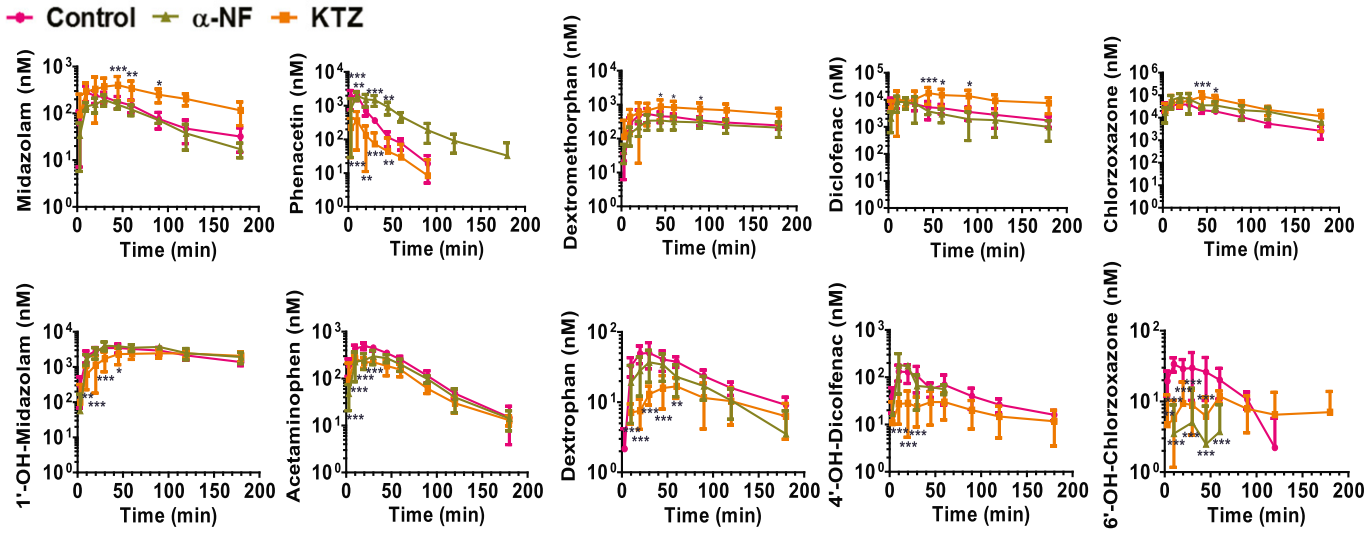

Fig. 2. Single-mouse PK profiles of multiple P450 probe drugs and corresponding metabolites: effects of known P450 inhibitors. Pretreatment with a single 50-mg/kg intraperitoneal dose of KTZ led to sharply increased systemic exposure to MDZ as well as significantly higher exposure to DIC and CLZ. By contrast, a single 100-mg/kg intraperitoneal dose of α-NF prior to cocktail administration caused much higher exposure to PHE ($P < 0.001$ for drug treatment and time). $^{*}P < 0.05$; $^{**}P < 0.01$; $^{***}P < 0.001$ at the indicated time points, compared with vehicle control (two-way analysis of variance with Bonferroni post hoc tests). Mice were pretreated intraperitoneally with KTZ, α-NF, or vehicle. One hour later, the cocktail drugs were administered via oral gavage (setting $t = 0$ minutes). Blood collection was carried out over 3–180 minutes. Values at individual time points represent means ± S.D. of six animals, as determined by LC-MS/MS assay. Missing data for some treatments at later time points were noted when analyte concentrations from all animals fell below the lower limits of quantification of the analytical assay.

mice were administered either the miR-34a agent or negative control (tRNA/MSA) using the same dosing scheme as described above. Twenty-four hours after the final dose, mice were anesthetized and liver tissues were harvested for microsomal preparation. A small piece of liver tissue from each mouse was stored in RNAlater (Sigma-Aldrich) at −80°C prior to RNA isolation.

LC-MS/MS Analysis of Cocktail Drugs and Corresponding Metabolites. Calibrators were prepared using blank CD-1 mouse plasma (with EDTA) and the appropriate concentrations of probe drugs and metabolites. Briefly, a 3-μl aliquot of calibrator or unknown plasma sample was added to 400 μl acetonitrile containing 5 nM of internal standards warfarin and harmaline in a 1.5-ml microcentrifuge tube. To precipitate proteins, the tube was vortexed for 30 seconds and centrifuged at 13,200 rpm and 4°C for 10 minutes. The supernatant was collected and dried over air at room temperature. The resulting residue was reconstituted with 60 μl 20% methanol in distilled water and centrifuged at 13,200 rpm and 4°C for 15 minutes to remove remaining debris prior to injection for LC-MS/MS analysis.

Drugs and metabolites were separated on a Zorbax C18 Eclipse Plus C18 reverse-phase LC column (2.1 × 50 mm, 3.5 μm; Agilent Technologies Inc., Santa Clara, CA) maintained at 35°C, using a Shimadzu Prominence Ultra-Fast LC system (Shimadzu Corporation, Kyoto, Japan) that consisted of binary pumps

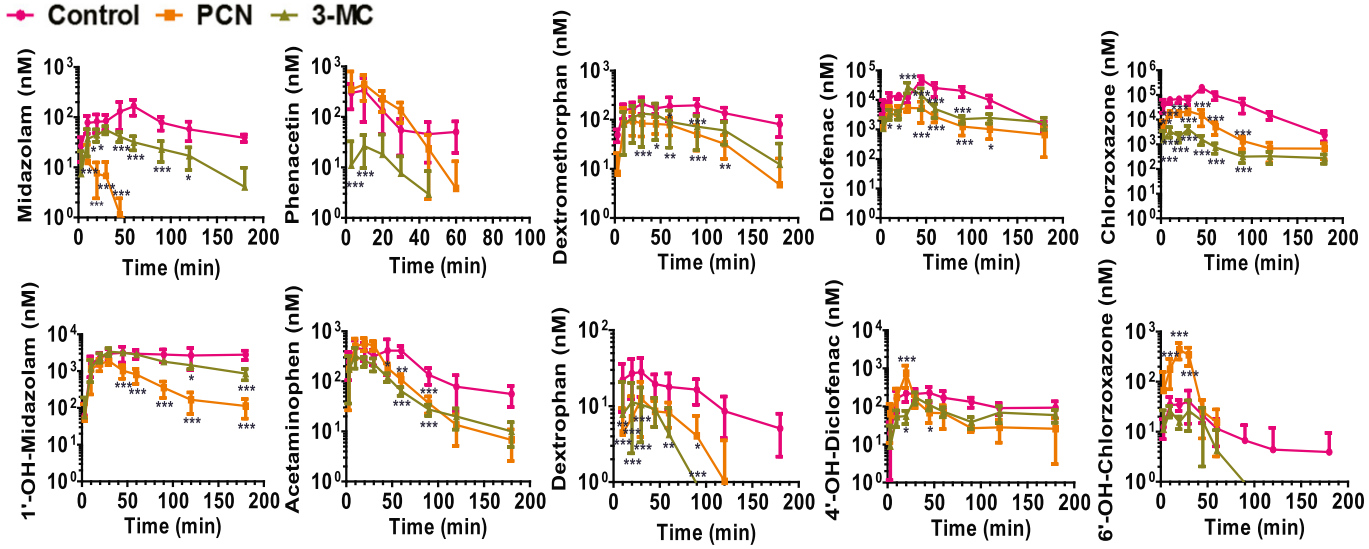

Fig. 3. Single-mouse PK profiles of multiple P450 probe drugs and corresponding metabolites: effects of known P450 inducers. Pretreatment with three 40-mg/kg intraperitoneal doses (24 hours apart) of PCN led to a remarkably lower exposure to MDZ and CLZ; similarly, three 50-mg/kg intraperitoneal doses of 3-MC sharply reduced the exposure to PHE, MDZ, and CLZ. A slight decrease in systemic exposure to DXM and DIC was also shown in PCN– and 3-MC–treated mice ($P < 0.001$ for drug treatment and time). $^{*}P < 0.05$; $^{**}P < 0.01$; $^{***}P < 0.001$ at the indicated time points, compared with vehicle control (two-way analysis of variance with Bonferroni post hoc tests). Mice were administered PCN, 3-MC, or vehicle (corn oil) intraperitoneally every day for 3 days. One day after the final dose, animals were administered the cocktail drugs by oral gavage (setting $t = 0$ minutes) and blood was collected over 3–180 minutes. Values represent means ± S.D. of six animals. Missing data for some treatments at later time points were noted when analyte concentrations from all animals fell below the lower limits of quantification of the analytical assay.

(LC-20AD), a degassing unit (LC-20A 3R), an autosampler (SIL-20AC HT), and a column oven (CTO-20AC). Mobile phases consisted of 100% water (A) and 100% methanol (B) supplemented with 0.1% formic acid [when used for electrospray ionization (ESI)-positive mode only]. A constant flow rate of 0.4 ml/min was used for separation. In ESI-positive ion mode for the detection of MDZ, DXM, PHE, and corresponding metabolites, the column was eluted with 10% B for 0.5 minutes, which was increased to 25% B over 1.5 minutes, then to 45% B over 5 minutes, and then held at 90% B for 2 minutes before it was returned to the initial condition for 3 minutes. In ESI-negative ion mode for the analyses of CLZ, DIC and corresponding metabolites, the column was eluted with 10% B for 1 minute, which was increased to 52% B over 2.5 minutes, held at 52% B for 1.5 minutes, and then held at 90% B for 1 minute before it was returned to initial conditions for 3 minutes.

Analytes were detected and quantified by multiple reaction monitoring using an AB Sciex 4000 QTRAP MS/MS system (AB Sciex, Framingham, MA) under optimal conditions as follows: ion spray voltage of 5.4 kV, desolvation temperature of 500°C curtain gas pressure of 30 psi, nebulizer and turbo gas pressures of 50 psi, and entrance potential of 10 V. Specific MS conditions for individual multiple reaction monitoring were optimized and are listed in Table 1. Each analyte peak area was normalized to the internal standard (harmaline for ESI-positive analytes, and warfarin for ESI-negative analytes). The calibration curve was generated for each analyte using Analyst software (version 1.6.2; AB Sciex). The accuracy and precision were further validated. In addition, after data analysis, analyte concentrations in a few test samples were revealed to be above the calibration ranges, which were accurately requantified after diluting the original plasma samples in blank CD-1 mouse plasma.

RNA Isolation and Quantification of Pre–miR-34a and Mature miR-34a. Total RNA was isolated using the Direct-zol RNA kit (Zymo Research, Irvine, CA), following the manufacturer's instructions. cDNA was generated by reverse transcription and levels of precursor and mature miR-34a were quantitated by corresponding selective real-time quantitative polymerase chain reaction assays on a CFX96 Touch real-time polymerase chain reaction system (Bio-Rad), as described previously (Wang et al., 2015). Cycle thresholds (Ct) for precursor and mature miR-34a were determined by regression, normalized to U6 small nucleolar RNA and then to the control using the $2^{-\Delta\Delta Ct}$ formula.

Mouse Liver Microsome Preparation and In Vitro Drug Metabolism Incubation. Mouse liver microsomes were prepared by following the standard protocol (Knights et al., 2016) and protein concentrations were determined using a BCA Protein Assay Kit (Thermo Fisher Scientific, Waltham, MA). To assay intrinsic clearance of P450 probe drugs, microsomes (final concentration of 0.5 μg microsomal protein/μl in each incubation) were preincubated with P450 cocktail (final concentration of 3 μM PHE, 2 μM DXM, 1 μM MDZ, 2 μM DIC, and 3 μM CLZ) in 0.1 M potassium phosphate buffer, pH 7.4, in a water bath for 5 minutes at 37°C. To initiate the reaction, NADPH (1-mM final concentration) was added and the reaction was quenched at different time points (0, 5, 10, and 20 minutes) with 3 ml ice-cold acetonitrile containing 10 μM harmaline and warfarin as internal standards. A negative control lacking NADPH was included alongside all samples and time points to determine enzymatic specificity and microsome quality. The mixture was vortexed and centrifuged at 10,000*g* for 10 minutes. Three milliliters of the supernatant was decanted and dried over air, and the residue was reconstituted with 100 μl 20% methanol. Levels of parent drugs and specific metabolites were quantitated using the LC-MS/MS methods described above.

PK Modeling. PK data analyses were conducted using a noncompartmental model (Kinetica, version 5.1; Thermo Fisher Scientific), which provided the estimation of corresponding PK parameters, including maximum concentration

TABLE 3

Effects of KTZ and α-NF on PK parameters of individual drugs and metabolites

Data were fit to a noncompartmental PK model. Values represent means ± S.D. generated from six mice.

Analyte	Treatment	C_{max} [b]	$AUC_{0\rightarrow\infty}$ [c]	Extrap	$t_{1/2}$	CL/F	V_z/F
				%	*h*	*l/h*	*liters*
Substrate							
MDZ	Control	290.8 ± 89.7	347.3 ± 91.2	10.00	0.858 ± 0.297	0.282 ± 0.080	0.357 ± 0.160
	KTZ	472.8 ± 214.9	978.2 ± 34.8***	22.17	1.26 ± 0.65	0.108 ± 0.047***	0.178 ± 0.065**
	α-NF	208.7 ± 51.3	258.0 ± 29.7	7.12	0.739 ± 0.174	0.361 ± 0.044	0.378 ± 0.070
PHE	Control	2.182 ± 0.851	613.7 ± 170.8	2.74	0.228 ± 0.055	0.803 ± 0.169	0.259 ± 0.064
	KTZ	0.775 ± 0.666*	207.1 ± 161.5	6.31	0.213 ± 0.123	5.03 ± 5.12	1.20 ± 0.91**
	α-NF	2.167 ± 0.445	1.454 ± 0.430***	1.93	0.440 ± 0.190**	0.344 ± 0.087	0.211 ± 0.081
DXM	Control	592.8 ± 226.0	1.596 ± 0.490	39.68	1.96 ± 0.45	14.4 ± 6.2	37.7 ± 8.6
	KTZ	974.0 ± 472.0	4.011 ± 2.324**	45.32	2.36 ± 0.46	6.40 ± 4.55	19.8 ± 12.0
	α-NF	381.0 ± 147.7	1.192 ± 0.651	34.13	1.76 ± 0.54	29.7 ± 22.7	62.7 ± 34.2
DIC	Control	9.247 ± 3.762	14.68 ± 7.06	20.57	1.21 ± 0.37	0.386 ± 0.152	0.634 ± 0.260
	KTZ	20.32 ± 10.45**	52.77 ± 27.62*	39.30	1.90 ± 0.43	0.0866 ± 0.106	0.200 ± 0.190
	α-NF	8.218 ± 4.138	9.786 ± 6.136	22.13	1.51 ± 0.86	0.553 ± 0.331	1.28 ± 0.59**
CLZ	Control	41.91 ± 11.47	45.03 ± 5.35	6.73	0.660 ± 0.237	1.12 ± 1.03	0.910 ± 0.651
	KTZ	109.5 ± 58.4**	119.5 ± 50.42**	13.2	0.767 ± 0.173	0.218 ± 0.104	0.228 ± 0.112**
	α-NF	71.29 ± 37.52	91.55 ± 30.90	7.40	0.688 ± 0.240	0.384 ± 0.216	0.329 ± 0.089
Metabolite							
1′-OH-MDZ	Control	3.758 ± 0.750	10.19 ± 1.89	28.73	1.49 ± 0.22		
	KTZ	2.992 ± 0.628	17.72 ± 9.03	58.95	3.70 ± 1.64*		
	α-NF	4.505 ± 0.491	13.27 ± 4.39	34.56	1.73 ± 0.53		
APAP	Control	500.0 ± 69.4	529.6 ± 59.5	1.86	0.475 ± 0.097		
	KTZ	381.5 ± 186.2	364.4 ± 384.3**	2.64	0.537 ± 0.087		
	α-NF	362.2 ± 140.7	379.2 ± 80.1*	3.11	0.529 ± 0.116		
DXO	Control	53.6 ± 19.4	87.9 ± 9.4	16.40	1.08 ± 0.45		
	KTZ	25.3 ± 10.7**	61.5 ± 19.2**	30.00	1.34 ± 0.21		
	α-NF	40.1 ± 14.3	56.6 ± 18.6	20.88	0.948 ± 0.33		
4′-OH-DIC	Control	141.6 ± 57.5	171.5 ± 56.3	14.61	1.09 ± 0.25		
	KTZ	36.4 ± 21.3*	97.8 ± 41.3**	30.05	1.56 ± 0.17**		
	α-NF[a]	180.8	8.4	3.20	2.10		
6-OH-CLZ	Control	43.33 ± 4.62	40.7 ± 10.4	16.77	0.526 ± 0.083		
	KTZ	16.47 ± 4.73***	51.4 ± 19.2	33.02	4.16 ± 1.72**		
	α-NF[a]	5.043	7.7	66.4	1.15		

Extrap, extrapolated contribution to AUC.

[a]Given incomplete data points because some were below quantification limits, a sparse data model was used.

[b]Values are given in nM for MDZ, DXM, APAP, DXO, 4′-OH-DIC, and 6-OH-CLZ and in μM for PHE, DIC, CLZ, and 1′-OH-MDZ.

[c]Values are given in nM·h for MDZ, PHE (control and KTZ) APAP, DXO, 4′-OH-DIC, and 6-OH-CLZ and in μM·h for PHE (α-NF), DXM, DIC, CLZ, and 1′-OH-MDZ.

*$P < 0.01$; **$P < 0.05$; ***$P < 0.001$ compared with the control (one-way analysis of variance with Bonferroni post hoc tests).

(C_{max}), elimination half-life ($t_{1/2}$), area under the plasma time curve ($AUC_{0\to\infty}$), extrapolated contribution to the AUC, oral clearance (CL/F), and apparent volume of distribution during the terminal elimination phase (V_z/F). In vitro substrate depletion data were fit to a monoexponential decay model (or biphasic decay for MDZ). In vitro intrinsic clearance (CL_{int}) was calculated using the equation $CL_{int} = A_0/AUC_{0\to\infty}$.

Statistical Analysis. Values represent means ± S.D. Drug and metabolite concentration versus time curves were compared for different treatments using two-way analysis of variance and Bonferroni post tests (GraphPad Prism software; GraphPad Inc., La Jolla, CA). PK parameters were further compared using one-way analysis of variance and Bonferroni post tests. Differences were considered statistically significant when the probability was less than 0.05 ($P < 0.05$).

Results

Validation of Single-Mouse PK Approach for DDI Studies. Lateral tail-vein puncture (Fig. 1) was found to be a practical means to manual microsampling, yielding up to 20 μl whole blood per time point. This procedure was found to cause minimal stress to the mice, and a maximum of 180 μl whole blood could be collected for nine time points over a 3-hour time period. Furthermore, after centrifugation and isolation of plasma, a small volume (3 μl) was found to be sufficient for LC-MS/MS quantification of multiple P450 probe drugs and corresponding metabolites under optimal MS conditions (Table 1). Calibrators that were within 15% variation were included to generate a calibration curve for each analyte, and all calibration curves showed excellent linearity ($R^2 \geq 0.99$) within the calibration ranges (Table 1). This LC-MS/MS assay provided accurate and precise quantification of both substrates and metabolites, with minimal intra- and interday variability (Table 2). As such, a complete PK profile was readily obtained after LC-MS/MS analyses of serial plasma samples obtained from a single mouse (data not shown; Figs. 2 and 3).

Single-Mouse PK Studies on Inhibition-Based DDIs. To evaluate the utility of this single-mouse PK method, we first examined the effects of KTZ and α-NF, two known P450 inhibitors, on the PK of individual P450 probe substrates in mice. The results showed that plasma MDZ concentrations were significantly increased in mice pretreated with KTZ, which was reflected by a 2- or 3-fold increase in both C_{max} and $AUC_{0\to\infty}$, respectively, lower oral clearance CL/F, and prolonged elimination $t_{1/2}$ (Table 3). This was also associated with significantly lower levels of 1′-OH-MDZ in mice pretreated with KTZ (Fig. 2; Table 3). By contrast, plasma MDZ and 1′-OH-MDZ concentrations and PK parameters were not significantly affected by α-NF pretreatment, with respect to the control (Fig. 2; Table 3).

Pretreatment with α-NF led to significantly higher plasma PHE concentrations in mice (Fig. 2), and this was reflected by a 2-fold increase in AUC and $t_{1/2}$ as well as a reduction in clearance by one-half (Table 3). Consistently, plasma APAP concentrations were significantly lower in mice pretreated with α-NF (Fig. 2), which was also indicated by significantly lower C_{max} and $AUC_{0\to\infty}$ values (Table 3). Interestingly, plasma PHE concentrations in KTZ-treated mice showed a general decrease compared with the control (Fig. 2), reflected in a significantly

TABLE 4

Effects of PCN and 3-MC on PK parameters of individual drugs and metabolites

Data were fit to a noncompartmental PK model. Values represent means ± S.D. generated from six mice.

	Treatment	C_{max}[b]	$AUC_{0\to\infty}$[c]	Extrap	$t_{1/2}$	CL/F	V_z/F
				%	*h*	*l/h*	*liters*
Substrate							
MDZ	Control	173.0 ± 53.7	321.5 ± 51.0	21.93	1.36 ± 0.27	0.288 ± 0.051	0.558 ± 0.113
	PCN[a]	16.06 ± 13.4*	13.1 ± 3.7	1.24	0.52[a]	3.8×10^{-5}	1.8×10^{3}
	3-MC	56.90 ± 11.8*	74.6 ± 32.5*	13.12	0.867 ± 0.274**	1.26 ± 0.45***	1.51 ± 0.63**
PHE	Control	425.8 ± 256.9	154.4 ± 93.3	18.37	0.466 ± 0.137	3.74 ± 1.57	2.52 ± 1.47
	PCN	550.0 ± 386.2	150.1 ± 68.4	10.64	0.155 ± 0.044***	3.24 ± 1.59	0.761 ± 0.589
	3-MC[a]	72.0	4.6	0.01	ND	ND	ND
DXM	Control	237.2 ± 88.2	646.9 ± 137.6	25.44	1.39 ± 0.36	39.6 ± 12.3	122 ± 85
	PCN	143.4 ± 60.6	213.0 ± 36.4***	30.84	1.09 ± 0.47	158 ± 57	220 ± 53
	3-MC	154.5 ± 97.9	42.3 ± 82.5***	27.14	1.20 ± 0.81	169 ± 121	206 ± 70
DIC	Control	49.15 ± 13.99	45.23 ± 14.39	1.78	0.418 ± 0.043	1.37 ± 0.97	0.797 ± 0.504
	PCN	6.592 ± 2.613*	7.23 ± 2.81*	12.32	0.979 ± 0.410**	2.05 ± 1.34	2.38 ± 1.17***
	3-MC	29.75 ± 9.12**	17.20 ± 4.8*	9.59	1.03 ± 0.33**	0.616 ± 0.390	0.801 ± 0.290
CLZ	Control	199.0 ± 61.9	153.3 ± 43.5	0.94	0.380 ± 0.062	1.93 ± 1.22	0.999 ± 0.565
	PCN	23.25 ± 6.91*	16.6 ± 4.9*	4.09	0.732 ± 0.314	4.02 ± 2.74	3.96 ± 2.02
	3-MC	4.645 ± 1.138*	3.18 ± 0.91*	7.09	1.04 ± 0.401***	9.06 ± 5.63**	11.6 ± 5.2*
Metabolite							
1′-OH-MDZ	Control	4.540 ± 0.449	11.88 ± 9.56	32.67	1.48 ± 0.88		
	PCN	1.950 ± 0.528**	1.81 ± 0.38**	6.66	0.672 ± 0.276		
	3-MC	3.532 ± 0.616**	7.46 ± 1.69	22.81	1.29 ± 0.43		
APAP	Control	523.6 ± 190.8	671.6 ± 237.6	8.59	0.820 ± 0.233		
	PCN	623.3 ± 140.5	367.8 ± 70.7**	1.85	0.467 ± 0.172**		
	3-MC	336.8 ± 139.0	225.8 ± 62.7***	3.81	0.702 ± 0.227		
DXO	Control	29.9 ± 14.8	56.3 ± 10.3	15.56	1.17 ± 0.38		
	PCN	15.8 ± 6.3	26.1 ± 8.7***	52.30	1.16 ± 0.43		
	3-MC	14.6 ± 9.6	20.8 ± 46.5***	18.66	0.376 ± 0.181		
4′-OH-DIC	Control	240.2 ± 90.0	631.1 ± 250.2	32.76	1.85 ± 0.34		
	PCN	747.5 ± 435.2**	315.6 ± 133.9**	14.77	1.28 ± 0.49		
	3-MC	173.3 ± 61.0	362.4 ± 151.7	43.10	2.56 ± 1.19		
6-OH-CLZ	Control	60.7 ± 51.8	31.9 ± 12.8	12.24	0.422 ± 0.135		
	PCN[a]	458.4 ± 134.1*	171.1*	0.01	0.357[a]		
	3-MC	33.7 ± 10.9	21.6 ± 2.8	37.70	0.620 ± 0.049		

Extrap, extrapolated contribution to AUC; ND, not determined due to insufficient data points representing the elimination phase.
[a]Given incomplete data points because some were below quantification limits, a sparse data model was used.
[b]Values are given in nM for MDZ, PHE, DXM, APAP, DXO, 4′-OH-DIC, and 6-OH-CLZ and in μM for DIC, CLZ, and 1′-OH-MDZ.
[c]Values are given in nM·h for MDZ, PHE, DXM, APAP, DXO, 4′-OH-DIC, and 6-OH-CLZ and in μM·h for DIC, CLZ, and 1′-OH-MDZ.
*$P < 0.001$; **$P < 0.05$; ***$P < 0.01$ compared with the control (one-way analysis of variance with Bonferroni post hoc tests).

decreased C_{max} and $AUC_{0\rightarrow\infty}$ and increased apparent volume of distribution V_z/F (Table 3). Nevertheless, mouse plasma APAP concentrations were not affected by KTZ treatment.

As expected, neither KTZ nor α-NF treatment had a significant impact on mouse plasma DXM concentrations and PK parameters (Fig. 2; Table 3). However, plasma DXO concentrations were significantly lower in KTZ-treated mice, particularly at earlier time points (Fig. 2), which was indicated by lower C_{max} and $AUC_{0\rightarrow\infty}$ values (Table 3). In addition, α-NF treatment did not alter DIC and CLZ PK in mice, whereas KTZ surprisingly caused a significant higher systemic exposure to DIC and CLZ (Fig. 2; Table 3). Inhibition of DIC and CLZ clearance was also associated with lower levels of exposure to their metabolites, 4′-OH-DIC and 6-OH-CLZ, respectively, in KTZ-treated mice (Fig. 2; Table 3).

Single-Mouse PK Studies on Induction-Based DDIs. We further employed this single-mouse PK method to investigate the effects of PCN and 3-MC, two known P450 inducers, on the PK of individual P450 probe substrates in mice. The results showed that plasma MDZ concentrations were sharply reduced in PCN-induced mice (Fig. 3), which was manifested by an 8-fold reduction in C_{max} values and 24-fold decrease in $AUC_{0\rightarrow\infty}$ values (Table 4). Surprisingly, plasma unconjugated 1′-OH-MDZ concentrations were not increased but decreased by almost 10-fold at later time points in PCN-treated mice, leading to a 6-fold lower $AUC_{0\rightarrow\infty}$ and a 2-fold lower $t_{1/2}$ value. In addition, pretreatment with 3-MC significantly decreased systemic exposure to MDZ compared with the control, whereas the degrees of change in PK parameters such as C_{max}, $AUC_{0\rightarrow\infty}$, and CL/F were reduced compared with PCN treatment (Fig. 3; Table 4).

Pretreatment with 3-MC remarkably reduced plasma PHE concentrations in mice compared with the control, whereas PCN showed minimal effects (Fig. 3). In particular, plasma PHE concentrations in 3-MC–treated animals were reduced by approximately 10-fold at all time points and then fell below the lowest limit of quantification (Table 1) at 45 minutes compared with 60 minutes for the control and PCN-treated groups, similar to the observation for MDZ in PCN-treated animals (Fig. 3). As such, there were 6- and 33-fold decreases in C_{max} and $AUC_{0\rightarrow\infty}$ values in 3-MC–treated mice (Table 4), respectively. Likewise, plasma unconjugated APAP concentrations were reduced in both PCN– and 3-MC–treated animals with respect to the control, although to a slightly greater degree in 3-MC–treated mice (Fig. 3; Table 4).

In addition, pretreatment with PCN and 3-MC significantly reduced plasma DXM, DIC, and CLZ concentrations in mice (Fig. 3), although to a lower degree than the effects of PCN on MDZ or 3-MC on PHE. This was also manifested by modest changes in PK parameters, including a decrease in C_{max} and $AUC_{0\rightarrow\infty}$ values as well as an increase in CL/F values (Table 4). However, the effects of PCN and 3-MC on unconjugated metabolite levels were relatively complex (Fig. 3). First, DXO concentrations were lower in PCN– and 3-MC–treated mice at all time points. Second, 4-OH-DIC concentrations were generally lower in 3-MC–treated mice at all time points, whereas they were higher in PCN-treated mice at an earlier stage (0–30 minutes) and were much lower at a later stage (30–180 minutes). Third, PCN treatment led to production of significantly higher levels of plasma 6-OH-CLZ concentrations in mice, whereas 3-MC showed minimal influence. These effects were consistently reflected in the changes in corresponding PK parameters such as C_{max}, $AUC_{0\rightarrow\infty}$, and $t_{1/2}$ (Table 4).

Effects of the Biologic miR-34a Agent on the PK of P450 Probe Drugs. After the validation of this single-mouse PK method through inhibition- and induction-based DDI studies, we examined the possible effect of miR-34a on the PK of individual P450 probe substrates in mice. As shown by the drug concentrations versus time profiles (Fig. 4) and PK parameters (Table 5), pretreatment with miR-34a had no or minimal effects on the PK of PHE, DXM, and CLZ as well as their corresponding metabolites but had a modest impact on the PK of MDZ and DIC. In particular, the $AUC_{0\rightarrow\infty}$ of MDZ was 60% higher in mice treated with miR-34a than the control, whereas its elimination $t_{1/2}$ and primary PK parameters were unaffected. Furthermore, there was no difference in 1′-OH-MDZ PK in mice treated with miR-34a and control RNA. Similarly, a higher C_{max} for DIC was observed in mice after miR-34a pretreatment (Fig. 4), leading to a 10% higher exposure ($AUC_{0\rightarrow\infty}$), which was not statistically significant (Table 5). Likewise, the PK of metabolite 4′-OH-DIC did not differ in mice treated with miR-34a and control RNA. These findings indicate that miR-34a seemed to have a marginal (<50%) effect on the PK of P450 probe drugs in mice compared with control RNA.

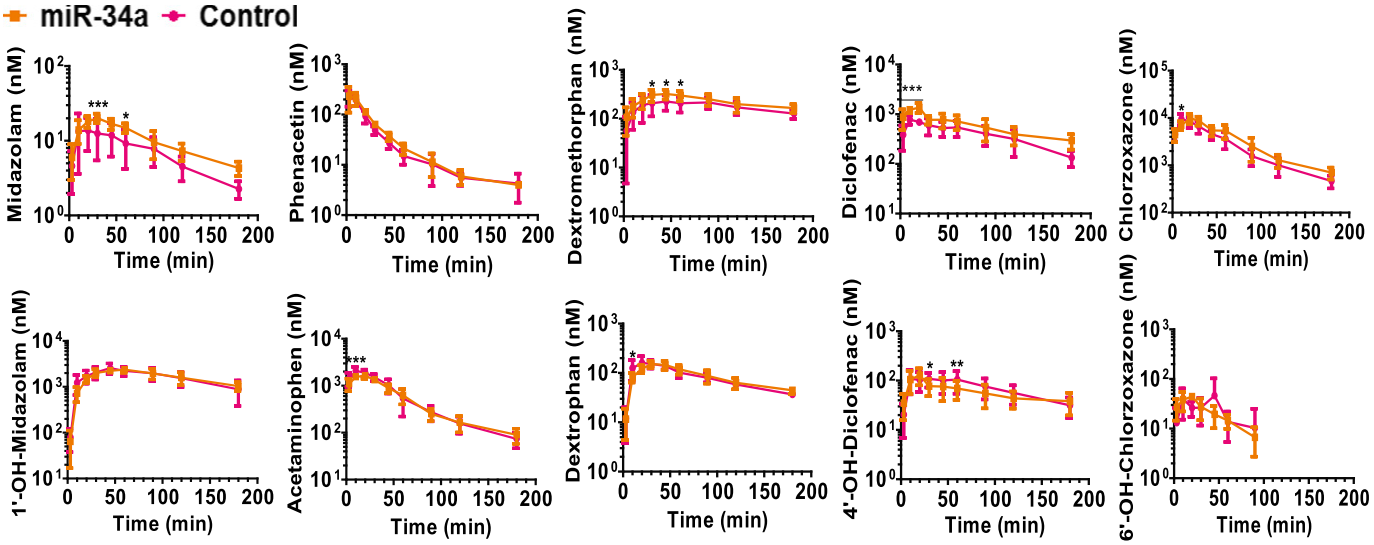

Fig. 4. Effects of miR-34a on PK profiles of individual P450 probe drugs and corresponding metabolites. Intravenous administration of miR-34a (15 μg/mouse, dosed four times over 4 days) to mice led to 45% and 48% increases in systemic exposure to MDZ and DIC, respectively. Mice were treated intravenously with miR-34a for 4 days, followed by oral administration of cocktail drugs. After a 2-week washout and recovery period, the same mice were pretreated intravenously with control tRNA/MSA for 4 days, followed by oral administration of the cocktail drugs. Individual data points represent means ± S.D. of six mice. *$P < 0.05$; **$P < 0.01$; ***$P < 0.001$ at the indicated time points, compared with control treatment (two-way analysis of variance with paired Bonferroni post hoc tests).

TABLE 5

Effects of miR-34a on the PK parameters of individual drugs and metabolites

Data were fit to a noncompartmental PK model. Values represent means ± S.D. generated from six mice.

	Treatment	C_{max}[a]	$AUC_{0\to\infty}$[b]	Extrap	$t_{1/2}$	CL/F	V_z/F
				%	*h*	*l/h*	*liters*
Substrate							
MDZ	Control	15.9 ± 8.9	23.4 ± 7.5	20.54	1.237 ± 0.710	6.995 ± 4.317	3.822 ± 1.115
	miR-34a	20.7 ± 3.0	37.4 ± 5.4*	17.72	1.182 ± 0.245	4.122 ± 0.897	2.432 ± 0.351
PHE	Control	229.0 ± 68.2	74.3 ± 14.6	13.27	0.256 ± 0.068	2.349 ± 0.981	6.243 ± 1.295
	miR-34a	225.7 ± 96.8	91.3 ± 13.8**	14.95	0.297 ± 0.044	2.166 ± 0.461	5.032 ± 0.708
DXM	Control	247.6 ± 88.1	906.6 ± 388.7	37.30	3.052 ± 2.771	70.33 ± 20.04	23.56 ± 14.11
	miR-34a	349.2 ± 74.8*	1276 ± 296***	49.15	2.762 ± 0.984	50.63 ± 11.41	13.81 ± 4.80
DIC	Control	841.0 ± 174.5	2.345 ± 1.768	30.09	1.832 ± 1.588	7.630 ± 5.150	5.067 ± 4.019
	miR-34a	1.448 ± 0.239*	2.612 ± 0.752	25.69	1.558 ± 0.480	4.094 ± 1.725	2.026 ± 1.058
CLZ	Control	9.856 ± 2.443	8.722 ± 1.248	4.16	0.644 ± 0.158	6.751 ± 3.613	8.152 ± 6.015
	miR-34a	10.73 ± 1.866	11.14 ± 1.80***	5.56	0.659 ± 0.153	4.328 ± 2.053	5.089 ± 3.450
Metabolite							
1′-OH-MDZ	Control	2.665 ± 0.566	7.807 ± 3.186	29.44	1.432 ± 0.553		
	miR-34a	2.443 ± 0.377	7.424 ± 1.275	32.67	1.630 ± 0.249		
APAP	Control	2.147 ± 0.395	1.797 ± 0.336	5.08	0.763 ± 0.265		
	miR-34a	1.700 ± 0.169**	1.640 ± 0.158	4.86	0.692 ± 0.154		
DXO	Control	175.6 ± 48.8	307.9 ± 41.7	22.18	1.271 ± 0.160		
	miR-34a	163.2 ± 16.7	358.9 ± 51.8	25.66	1.417 ± 0.144		
4′-OH-DIC	Control	136.5 ± 51.4	275.6 ± 105.8	20.94	1.286 ± 0.372		
	miR-34a	126.0 ± 48.9	284.5 ± 127.1	33.77	1.984 ± 0.656		
6-OH-CLZ	Control	45.57 ± 0.02	42.2 ± 11.6	25.77	0.629 ± 0.352		
	miR-34a	47.50 ± 0.01	40.0 ± 5.5	17.75	0.684 ± 0.150		

Extrap, extrapolated contribution to AUC.

[a]Values are given in nM for MDZ, PHE, DXM, DIC (control), DXO, 4′-OH-DIC, and 6-OH-CLZ and in μM for DIC (miR-34a), CLZ, 1′-OH-MDZ, and APAP.

[b]Values are given in nM·h for MDZ, PHE, DXM, DXO, 4′-OH-DIC, and 6-OH-CLZ and in μM·h for DIC, CLZ, 1′-OH-MDZ, and APAP.

*$P < 0.001$; **$P < 0.01$; ***$P < 0.05$ compared with the control (one-way analysis of variance with paired Bonferroni post hoc tests).

We found that the levels of precursor and mature miR-34a were increased by approximately 10- and 80-fold, respectively, in mouse livers treated with the biologic miR-34a prodrug (Fig. 5A), which indicates hepatic accumulation of pre–miR-34a and production of mature miR-34a. In addition, time-dependent substrate depletion was found to be minimally altered by liver microsomes prepared from the mice treated with an miR-34a agent, compared with the control (Fig. 5B, Table 6). Notably, DXM depletion (CL_{int}) was attenuated by approximately 30% in liver microsomes derived from miR-34a–treated mice. Finally, the depletion of DIC and CLZ was minimal in mouse liver microsomes prepared from both groups (Fig. 5B, Table 6), and both were indistinguishable from the NADPH-null reaction controls (data not shown), which agree with their metabolic stabilities in liver microsomes.

Discussion

With the development of new carriers for the delivery of nucleic acids, many RNA agents have entered clinical trials as drug candidates (Ho and Yu, 2016). Because some miRNAs regulate genes underlying drug metabolism and disposition (Yu, 2009; Ingelman-Sundberg et al., 2013; Yokoi and Nakajima, 2013; Yu et al., 2016), it is essential to evaluate possible DDIs in vivo for safety reasons. Recently, our group engineered a biologic miR-34a prodrug whose mechanistic actions on target gene expression and xenograft tumor progression have been documented (Wang et al., 2015; Zhao et al., 2015, 2016). In this study, we elucidated the effects of biologic miR-34a on the PK of five P450 probe drugs after we established and validated a general, rapid, and practical single-mouse PK approach. Our results demonstrated a rather marginal (45%–48%) influence of miR-34a on systemic exposure to MDZ and DIC in mouse models, as well as the lack of effects on the PK of DXM, PHE, and CLZ.

This single-mouse PK approach involves a simple nonterminal, manual serial microsampling procedure, although it requires a sensitive and accurate LC-MS/MS analytical assay. Tail-vein blood collection is proven to be a reliable means for PK studies in rodents. A thorough comparison of PKs of six marketed drugs in rats using tail-vein, cannula and retro-orbital bleeding methods demonstrated that there were no or minor differences in PK properties among these blood sampling methods (Hui et al., 2007). Although one study reported statistically significant differences in gabapentin PK parameters (e.g., oral bioavailability: 46.82% ± 19.45% versus 61.54% ± 21.23%) in rats for manual and automated blood sampling methods (Aryal et al., 2011) and the latter procedures could be less stressful to mice (Teilmann et al., 2014), the actual 1.3-fold difference was rather marginal. Most importantly, the plasma drug concentrations versus time curves and estimated PK parameters using this single-mouse PK approach were equally or less variable than those studies using "giant rat" models (Granvil et al., 2003; Shen et al., 2011; Jiang et al., 2013), and variabilities shown in single-mouse PK studies should represent true differences among individual subjects.

The robustness and application of this single-mouse PK approach is demonstrated by the degrees of mechanistic DDIs between selective P450 inhibitors/inducers and corresponding P450 probe drugs in CD-1 mice. Supporting this, we found that pretreatment with α-NF led to a 2.3-fold increase in systemic exposure to PHE, and pretreatment with 3-MC resulted in a 33-fold decrease in exposure to PHE, which are in general agreement with those values identified using rat models (Table 7), although variable drug dosing regimens and animal models may provide some explanations for interstudy variations. The 2.8-fold increase in systemic exposure to MDZ in a single dose of KTZ-treated CD-1 mice revealed in this study is also close to the 3.3-fold increase defined in FVB/N mice (Granvil et al., 2003), given some rather minor differences in the stains of mice, doses of KTZ and MDZ, routes of administration, and dosing intervals (Table 7). Interstudy variations are also obvious for the degrees of DDIs between MDZ and KTZ in humans, where a single dose of KTZ showed reasonably less impact on MDZ exposure compared with multiple doses of KTZ (Table 7). Furthermore, the sharp change in MDZ exposure (25-fold decrease) in PCN-treated mice defined by the single-mouse PK approach in this study supports the

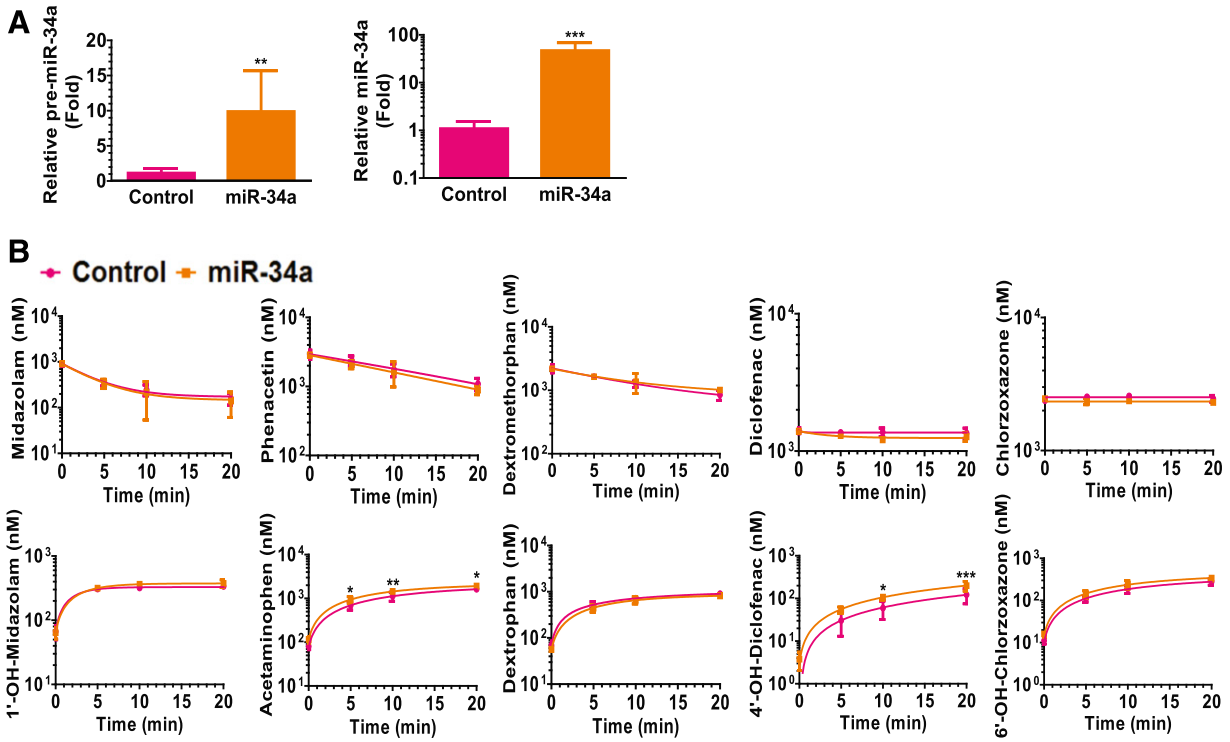

Fig. 5. Clearance of P450 probe drugs by liver microsomes prepared from mice treated with miR-34a and control RNA. (A) Precursor and mature miR-34a levels were significantly higher in liver tissues of mice treated with the bioengineered miR-34a prodrug. Mature miR-34a and pre–miR-34a were quantitated by selective qPCR assays and normalized to U6. (B) Comparison of the activities of mouse liver microsomes in the clearance of P450 probe drugs. Mice (five per treatment group) were treated intravenously with miR-34a or control RNA for 4 days. Total RNA and microsomes were prepared from dissected liver tissues for qPCR and in vitro metabolism experiments, respectively. Values represent means ± S.D. (n = 5 per group). *$P < 0.05$; **$P < 0.01$; ***$P < 0.001$ at indicated time points, compared with control (A, unpaired t test; B, two-way analysis of variance with Bonferroni post hoc tests). qPCR, quantitative polymerase chain reaction.

selectivity of PCN to induce murine drug-metabolizing enzymes via activation of the murine pregnane X receptor and the critical role of intestinal enzymes in the control of PK of orally administered MDZ (McCrea et al., 1999; Tsunoda et al., 1999; Granvil et al., 2003; Lam et al., 2003; Pang et al., 2011). Finally, because phase 2 conjugation metabolites are not monitored using this assay, a significant decrease, rather than increase, in plasma 1′-OH-MDZ concentration was observed in mice administered PCN. This is most likely explained by further conjugations of 1′-OH-MDZ, as mouse UDP-glucuronosyltransferases are inducible after PCN-mediated activation of the pregnane X receptor (Buckley and Klaassen, 2009).

The effects of P450 inducers (PCN and 3-MC), as well as P450 inhibitors (KTZ and α-NF), on the PK properties of parent probe drugs (e.g., MDZ and PHE) revealed in this study not only highlight the importance of corresponding murine P450 enzymes in the metabolism of these drugs but also illustrate some species differences. For example, lower levels of DDIs between KTZ and MDZ in mice than humans (Table 7) may be in part due to the significant contribution of Cyp2c enzymes to MDZ 1′-hydroxylation in mice (Perloff et al., 2000). In addition, we observed an approximately equal level of decrease in APAP exposure in KTZ– and α-NF–treated mice, whereas substrate drug PHE concentrations were decreased in KTZ-treated mice and increased in α-NF–treated mice. Likewise, a nearly equal significant decrease in APAP exposure was found in both PCN– and 3-MC–treated mice, whereas PHE concentrations were only decreased in 3-MC–treated mice. Although the exact mechanisms are unknown, the decrease in APAP may be partially due to complex changes in phase 2 conjugations after PHE *O*-de-ethylation, as well as the involvement of various P450 enzymes in APAP metabolism (Patten et al., 1993; Zaher et al., 1998). The observed increase in exposure to DIC by KTZ (Fig. 2) may be interpreted by the fact that DIC is oxidized not only by Cyp2c enzymes but also by other P450 isoforms, including Cyp3a in mice (Tang et al., 1999; Scheer et al., 2012). In addition, DXO formation was decreased approximately 2-fold in KTZ-treated mice and DXM PK was co-incidentally altered, which may reflect a modest inhibition of murine DXM *O*-demethylase Cyp2d enzymes by KTZ (Yu and Haining, 2006).

Using this single-mouse PK approach and a biologic miR-34a agent, rather than synthetic miRNA reagents bearing extensive artificial modifications (Duan and Yu, 2016; Ho and Yu, 2016), we were able to identify the somewhat limited effects of miR-34a on the PK of individual P450 probe drugs; this was also supported by findings from an in vitro metabolism study. Compared with control RNA treatment, miR-34a either did not affect (e.g., DXM, PHE, and CLZ exposure) or led to

TABLE 6

Effects of miR-34a on in vitro intrinsic clearance of P450 probe substrates

Values represent means ± S.D. (n = 5 per group).

Substrate	Treatment	$t_{1/2}$	CL_{int}
		min	*ml/min per mg protein*
MDZ	Control	2.52 ± 0.26	0.20 ± 0.04
	miR-34a	2.60 ± 0.34	0.24 ± 0.08
PHE	Control	14.62 ± 6.27	0.09 ± 0.02
	miR-34a	12.56 ± 2.19	0.11 ± 0.01
DXM	Control	14.34 ± 2.55	0.10 ± 0.01
	miR-34a	18.49 ± 1.38*	0.07 ± 0.01*

DXM intrinsic clearance was marginally attenuated in liver microsomes derived from mice treated with miR-34a agent, compared with the control. Data were fit to a monoexponential decay model (or biphasic decay for MDZ) to derive $t_{1/2}$ and CL_{int}. DIC and CLZ data are not fit to any model because there was minimal substrate depletion.

**$P < 0.01$.

TABLE 7

Comparison of the degrees of interactions between several paired drugs in various species using different dosing regimens

Substrate	Inhibitor or Inducer	Change of AUC	Dosing Regimen	Species	Reference
MDZ	KTZ	16-fold increase	3 doses of 200 mg KTZ every 12 h, p.o.; 90 min after last dose of KTZ, 6 mg MDZ plus 200 mg KTZ, p.o.	Humans	Tsunoda et al., 1999
		7.7-fold increase	200 mg KTZ for 12 days, p.o.; 1 h after the last dose of KTZ, 10 mg MDZ, p.o.	Humans	Lam et al., 2003
		5.0-fold increase	200 mg KTZ, p.o.; 2 h later, 2 mg MDZ, p.o.	Humans	McCrea et al., 1999
		6.5-fold increase	10 mg/kg KTZ, i.p.; 30 min later, 15 mg/kg MDZ, i.g.; 180 min later, 5 mg/kg KTZ, i.p., to maintain serum KTZ concentrations at $\geq$2 μg/ml	Sprague-Dawley rats	Kotegawa et al., 2002
		1.5-fold increase	10 mg/kg KTZ, i.p.; 30 min later, 5 mg/kg MDZ, i.v.; 180 min later, 5 mg/kg KTZ, i.p., to maintain serum KTZ concentrations at $\geq$2 μg/ml	Sprague-Dawley rats	Kotegawa et al., 2002
		3.3-fold increase	40 mg/kg KTZ, p.o.; 45 min later, 2.5 mg/kg MDZ, p.o.	FVB/N mice	Granvil et al., 2003
		6.3-fold increase	40 mg/kg KTZ, p.o.; 45 min later, 2.5 mg/kg MDZ, p.o.	CYP3A4-humanized FVB/N mice	Granvil et al., 2003
		2.8-fold increase	50 mg/kg KTZ, i.p.; 1 h later, 1 mg/kg MDZ in a cocktail, p.o.	CD-1 mice	This study
	PCN	10% increase	10 mg/kg PCN for 3 days, i.g.; 0.3 mg/kg MDZ, i.v.	C57BL/6J mice	Pang et al., 2011
		25-fold decrease	40 mg/kg PCN for 3 days, i.p.; 1 mg/kg MDZ in a cocktail, p.o.	CD-1 mice	This study
PHE	α-NF	1.8-fold increase	7 mg/kg α-NF, i.v.; 15 min later, 5 mg/kg PHE, i.v.	Sprague-Dawley rats	Zhuang et al., 2013
		2.3-fold increase	100 mg/kg α-NF, i.p.; 1 h later 2.8 mg/kg PHE in a cocktail, p.o.	CD-1 mice	This study
	3-MC	4.9-fold decrease	20 mg/kg 3-MC for 2 days, p.o.; 20 mg/kg PHE, i.v.	Wistar rats	Klippert et al., 1983
		13-fold decrease	20 mg/kg 3-MC for 2 days, p.o.; 20 mg/kg PHE, i.d.	Wistar rats	Klippert et al., 1983
		33-fold decrease	50 mg/kg 3-MC for 3 days, i.p.; 2.8 mg/kg PHE in a cocktail, p.o.	CD-1 mice	This study

minor (<50%) changes (e.g., MDZ and DIC). Compared with controls, DIC C_{max} and MDZ $AUC_{0\rightarrow\infty}$ values in miR-34a–treated mice were significantly increased (Table 5), suggesting a possible alteration of murine Cyp3a and Cyp2c by miR-34a. This is complementary to studies that found a negative correlation between miR-34a and CYP3A4 and CYP2C19 (Lamba et al., 2014), as well as miR-34a targeting of RXRα/NR2B1 (Oda et al., 2014) and Nrf2/NFE2L2 (Huang et al., 2014) by miR-34a. In addition, the HNF4α transcription factor was found to be highly conserved between mouse and human species (Boj et al., 2009) and miRNA recognition elements were identified for miR-34a in both the human and mouse 3′ untranslated region of HNF4α mRNA (Takagi et al., 2010) [three miR-34a miRNA recognition elements within the murine Rxra 3′ untranslated region by TargetScan (http://www.targetscan.org) and miRanda (http://www.microrna.org)].

Our findings from mouse models are also complicated by the presence of species differences in the expression of regulatory factors and drug-metabolizing enzymes and transporters, as well as their functions in drug processing. Indeed, we found that the formation of both 1′-OH-MDZ and 4′-OH-DIC was not altered in vivo (Table 5), nor was CL_{int} of either parent drug affected in vitro (Table 6). These data suggest that miR-34a–induced alterations of MDZ or DIC PK are not manifested in the alteration of murine P450 enzymes. In addition, DIC and CLZ depletion in mouse liver microsomes (Fig. 5B) was minimal, which not only supports their metabolic stability in microsomes but also suggests the presence of other mechanisms that are responsible for their clearance besides hepatic microsomal metabolism. As such, the discrepancy between the observed alterations to in vivo PK and in vitro probe drug clearance may be explained by modulation of phase 2 enzyme or drug transporter genes by miR-34a. Indeed, RXRα, a putative miR-34a target, likely modulates the expression of several glutathione *S*-transferase isoforms (Dai et al., 2005), although no similar evidence currently exists for sulfo- or glucuronosyltransferase enzymes.

In summary, this study established a practical approach to perform single-mouse PK and DDI studies, which was employed to demonstrate the remarkable PK DDIs between selective P450 inhibitors/inducers and P450 probe drugs in mice, as well as some species differences. In addition, we were able to reveal the marginal effects of miR-34a on MDZ, DIC, and DXM PK in mice. However, further research is required to confirm these findings, particularly in a more translational humanized mouse model.

Acknowledgments

The authors thank Pui Yan Ho, Meijuan Tu, and Cindy McReynolds for assistance in processing blood samples during the PK studies.

Authorship Contributions

Participated in research design: Jilek, Tian, Yu.
Conducted experiments: Jilek, Tian.
Performed data analysis: Jilek, Tian.
Wrote or contributed to the writing of the manuscript: Jilek, Tian, Yu.

References

Ambros V (2004) The functions of animal microRNAs. *Nature* **431**:350–355.
Aryal B, Tae-Hyun K, Yoon-Gyoon K, and Hyung-Gun K (2011) A comparative study of the pharmacokinetics of traditional and automated dosing/blood sampling systems using gabapentin. *Indian J Pharmacol* **43**:262–269.
Bader AG (2012) miR-34 - a microRNA replacement therapy is headed to the clinic. *Front Genet* **3**:120.
Bader AG, Brown D, and Winkler M (2010) The promise of microRNA replacement therapy. *Cancer Res* **70**:7027–7030.
Boj SF, Servitja JM, Martin D, Rios M, Talianidis I, Guigo R, and Ferrer J (2009) Functional targets of the monogenic diabetes transcription factors HNF-1alpha and HNF-4alpha are highly conserved between mice and humans. *Diabetes* **58**:1245–1253.
Buckley DB and Klaassen CD (2009) Induction of mouse UDP-glucuronosyltransferase mRNA expression in liver and intestine by activators of aryl-hydrocarbon receptor, constitutive androstane receptor, pregnane X receptor, peroxisome proliferator-activated receptor alpha, and nuclear factor erythroid 2-related factor 2. *Drug Metab Dispos* **37**:847–856.
Dai G, Chou N, He L, Gyamfi MA, Mendy AJ, Slitt AL, Klaassen CD, and Wan YJ (2005) Retinoid X receptor alpha regulates the expression of glutathione S-transferase genes and modulates acetaminophen-glutathione conjugation in mouse liver. *Mol Pharmacol* **68**:1590–1596.
Duan Z and Yu AM (2016) Bioengineered non-coding RNA agent (BERA) in action. *Bioengineered* **7**:411–417.
Granvil CP, Yu AM, Elizondo G, Akiyama TE, Cheung C, Feigenbaum L, Krausz KW, and Gonzalez FJ (2003) Expression of the human CYP3A4 gene in the small intestine of transgenic mice: in vitro metabolism and pharmacokinetics of midazolam. *Drug Metab Dispos* **31**:548–558.
Ho PY and Yu AM (2016) Bioengineering of noncoding RNAs for research agents and therapeutics. *Wiley Interdiscip Rev RNA* **7**:186–197.
Huang X, Gao Y, Qin J, and Lu S (2014) The role of miR-34a in the hepatoprotective effect of hydrogen sulfide on ischemia/reperfusion injury in young and old rats. *PLoS One* **9**:e113305.
Hui YH, Huang NH, Ebbert L, Bina H, Chiang A, Maples C, Pritt M, Kern T, and Patel N (2007) Pharmacokinetic comparisons of tail-bleeding with cannula- or retro-orbital bleeding techniques in rats using six marketed drugs. *J Pharmacol Toxicol Methods* **56**:256–264.
Ingelman-Sundberg M, Zhong XB, Hankinson O, Beedanagari S, Yu AM, Peng L, and Osawa Y (2013) Potential role of epigenetic mechanisms in the regulation of drug metabolism and transport. *Drug Metab Dispos* **41**:1725–1731.

Jiang XL, Shen HW, Mager DE, and Yu AM (2013) Pharmacokinetic interactions between monoamine oxidase A inhibitor harmaline and 5-methoxy-N,N-dimethyltryptamine, and the impact of CYP2D6 status. *Drug Metab Dispos* **41**:975–986.

Kasinski AL and Slack FJ (2011) Epigenetics and genetics. MicroRNAs en route to the clinic: progress in validating and targeting microRNAs for cancer therapy. *Nat Rev Cancer* **11**:849–864.

Klippert PJ, Littel RJ, and Noordhoek J (1983) In vivo O-de-ethylation of phenacetin in 3-methylcholanthrene-pretreated rats: gut wall and liver first-pass metabolism. *J Pharmacol Exp Ther* **225**:153–157.

Knights KM, Stresser DM, Miners JO, and Crespi CL (2016) In vitro drug metabolism using liver microsomes. *Curr Protoc Pharmacol* **74**:7.8.1–7.8.24.

Kotegawa T, Laurijssens BE, Von Moltke LL, Cotreau MM, Perloff MD, Venkatakrishnan K, Warrington JS, Granda BW, Harmatz JS, and Greenblatt DJ (2002) In vitro, pharmacokinetic, and pharmacodynamic interactions of ketoconazole and midazolam in the rat. *J Pharmacol Exp Ther* **302**:1228–1237.

Lam YW, Alfaro CL, Ereshefsky L, and Miller M (2003) Pharmacokinetic and pharmacodynamic interactions of oral midazolam with ketoconazole, fluoxetine, fluvoxamine, and nefazodone. *J Clin Pharmacol* **43**:1274–1282.

Lamba V, Ghodke Y, Guan W, and Tracy TS (2014) microRNA-34a is associated with expression of key hepatic transcription factors and cytochromes P450. *Biochem Biophys Res Commun* **445**: 404–411.

McCrea J, Prueksaritanont T, Gertz BJ, Carides A, Gillen L, Antonello S, Brucker MJ, Miller-Stein C, Osborne B, and Waldman S (1999) Concurrent administration of the erythromycin breath test (EBT) and oral midazolam as in vivo probes for CYP3A activity. *J Clin Pharmacol* **39**: 1212–1220.

Oda Y, Nakajima M, Tsuneyama K, Takamiya M, Aoki Y, Fukami T, and Yokoi T (2014) Retinoid X receptor α in human liver is regulated by miR-34a. *Biochem Pharmacol* **90**:179–187.

Pang X, Cheng J, Krausz KW, Guo DA, and Gonzalez FJ (2011) Pregnane X receptor-mediated induction of Cyp3a by black cohosh. *Xenobiotica* **41**:112–123.

Patten CJ, Thomas PE, Guy RL, Lee M, Gonzalez FJ, Guengerich FP, and Yang CS (1993) Cytochrome P450 enzymes involved in acetaminophen activation by rat and human liver microsomes and their kinetics. *Chem Res Toxicol* **6**:511–518.

Perloff MD, von Moltke LL, Court MH, Kotegawa T, Shader RI, and Greenblatt DJ (2000) Midazolam and triazolam biotransformation in mouse and human liver microsomes: relative contribution of CYP3A and CYP2C isoforms. *J Pharmacol Exp Ther* **292**:618–628.

Scheer N, Kapelyukh Y, Chatham L, Rode A, Buechel S, and Wolf CR (2012) Generation and characterization of novel cytochrome P450 Cyp2c gene cluster knockout and CYP2C9 humanized mouse lines. *Mol Pharmacol* **82**:1022–1029.

Shen HW, Jiang XL, and Yu AM (2011) Nonlinear pharmacokinetics of 5-methoxy-N,N-dimethyltryptamine in mice. *Drug Metab Dispos* **39**:1227–1234.

Takagi S, Nakajima M, Kida K, Yamaura Y, Fukami T, and Yokoi T (2010) MicroRNAs regulate human hepatocyte nuclear factor 4alpha, modulating the expression of metabolic enzymes and cell cycle. *J Biol Chem* **285**:4415–4422.

Tang W, Stearns RA, Bandiera SM, Zhang Y, Raab C, Braun MP, Dean DC, Pang J, Leung KH, Doss GA, et al. (1999) Studies on cytochrome P-450-mediated bioactivation of diclofenac in rats and in human hepatocytes: identification of glutathione conjugated metabolites. *Drug Metab Dispos* **27**:365–372.

Teilmann AC, Kalliokoski O, Sørensen DB, Hau J, and Abelson KS (2014) Manual versus automated blood sampling: impact of repeated blood sampling on stress parameters and behavior in male NMRI mice. *Lab Anim* **48**:278–291.

Tsunoda SM, Velez RL, von Moltke LL, and Greenblatt DJ (1999) Differentiation of intestinal and hepatic cytochrome P450 3A activity with use of midazolam as an in vivo probe: effect of ketoconazole. *Clin Pharmacol Ther* **66**:461–471.

Wang WP, Ho PY, Chen QX, Addepalli B, Limbach PA, Li MM, Wu WJ, Jilek JL, Qiu JX, Zhang HJ, et al. (2015) Bioengineering novel chimeric microRNA-34a for prodrug cancer therapy: high-yield expression and purification, and structural and functional characterization. *J Pharmacol Exp Ther* **354**:131–141.

Yokoi T and Nakajima M (2013) microRNAs as mediators of drug toxicity. *Annu Rev Pharmacol Toxicol* **53**:377–400.

Yu AM (2009) Role of microRNAs in the regulation of drug metabolism and disposition. *Expert Opin Drug Metab Toxicol* **5**:1513–1528.

Yu AM and Haining RL (2006) Expression, purification, and characterization of mouse CYP2d22. *Drug Metab Dispos* **34**:1167–1174.

Yu AM, Tian Y, Tu MJ, Ho PY, and Jilek JL (2016) MicroRNA pharmacoepigenetics: post-transcriptional regulation mechanisms behind variable drug disposition and strategy to develop more effective therapy. *Drug Metab Dispos* **44**:308–319.

Zaher H, Buters JT, Ward JM, Bruno MK, Lucas AM, Stern ST, Cohen SD, and Gonzalez FJ (1998) Protection against acetaminophen toxicity in CYP1A2 and CYP2E1 double-null mice. *Toxicol Appl Pharmacol* **152**:193–199.

Zhao Y, Tu MJ, Wang WP, Qiu JX, Yu AX, and Yu AM (2016) Genetically engineered pre-microRNA-34a prodrug suppresses orthotopic osteosarcoma xenograft tumor growth via the induction of apoptosis and cell cycle arrest. *Sci Rep* **6**:26611.

Zhao Y, Tu MJ, Yu YF, Wang WP, Chen QX, Qiu JX, Yu AX, and Yu AM (2015) Combination therapy with bioengineered miR-34a prodrug and doxorubicin synergistically suppresses osteosarcoma growth. *Biochem Pharmacol* **98**:602–613.

Zhuang XM, Zhong YH, Xiao WB, Li H, and Lu C (2013) Identification and characterization of psoralen and isopsoralen as potent CYP1A2 reversible and time-dependent inhibitors in human and rat preclinical studies. *Drug Metab Dispos* **41**:1914–1922.

Address correspondence to: Ai-Ming Yu, Department of Biochemistry and Molecular Medicine, University of California Davis School of Medicine, 2700 Stockton Boulevard, Room 2132, Sacramento, CA 95817. E-mail: aimyu@ucdavis.edu